Time Evolution of Surface Relief Structures in Thin Block Copolymer Films

A. Horvat, A. Knoll,† G. Krausch, and L. Tsarkova*

Physikalische Chemie II, Universität Bayreuth, 95440 Bayreuth, Germany

K. S. Lyakhova

Polymer Physics, Eindhoven University of Technology, PO Box 513, 5600 MB Eindhoven, The Netherlands

G. J. A. Sevink*

Soft Condensed Matter Group, Leiden Institute of Chemistry, Leiden University, 2300 RA Leiden, The Netherlands

A. V. Zvelindovsky*

Centre for Materials Science, Department of Physics, Astronomy and Mathematics, University of Central Lancashire, Preston, PR1 2HE, United Kingdom

R. Magerle

Chemische Physik, Technische Universität Chemnitz, 09107 Chemnitz, Germany

Received May 16, 2007; Revised Manuscript Received June 25, 2007

ABSTRACT: The dynamics of early stage of terrace formation in thin supported films of cylinder forming triblock copolymers was studied both theoretically using self-consistent-field theory (DSCFT) and experimentally by in-situ scanning force microscopy (SFM). In experiment, an initially flat film of incommensurable thickness was imaged continuously, and the evolution of a vertical orientation of cylinders into a parallel one as well as the respective development of thickness gradient (terrace formation) was captured in detail. On the grounds of these experimental observations, the parameters of the computational model $A_3B_{12}A_3$ were determined to match the structures in experiment. Both systems show excellent agreement in details of structural phase transitions and in the dynamics of the step development, suggesting that the underlying transport mechanisms are governed by diffusion. The early stage of terrace formation is characterized by the development of the step height up to 80% of its equilibrium value and associated reorientation of cylindrical domains.

1. Introduction

Block copolymers belong to the class of ordered fluids, which self-assemble into microdomains with characteristic lengths ranging from 10 to 100 nm. The morphology type and the characteristic dimensions are controlled by the block copolymer composition, the interaction between the blocks, and the total chain length N.[1]

The specific behavior of block copolymers in thin films is primarily dictated by the enhanced role of surface/interfacial energetics as well as by the interplay between the characteristic block copolymer spacings and the film thickness.[2−5] Preferential attraction of one of the blocks to the surface breaks the symmetry of the structure and favors layering of microdomains parallel to the surface plane through the entire film thickness. As a result, the energetically favored film thicknesses are then quantized with the characteristic structure period in the bulk (denoted here as c_0 for cylinder-forming block copolymers). The surface topography depends on the initial film thickness h_0 of as-cast substrate-supported film. When h_0 deviates from nc_0 (for symmetric wetting conditions), topographical features of macroscopic size such as islands, holes, or bicontinuous patterns with two distinct thicknesses nc_0 and $(n + 1)c_0$ are formed to satisfy the thickness constraint. Experimentally, nucleation and subsequent growth of surface relief structures, also called *terrace formation*, have been investigated mostly for lamellar systems as a function of surface fields,[6−8] molecular architecture,[9] film thickness,[10,11] and annealing conditions.[9,11,12] The coarsening of the surface macrodomains is typically followed by time-resolved optical micrographs or surface force microscopy (SFM) topographs, and the averaged macrodomain radius as a function of annealing conditions is determined. The development of surface roughness on an initially smooth film starts already during the early stages of annealing. The terrace heights continuously change with time until the commensurable thicknesses are achieved. The difference in the neighboring terraces heights up to 80% of its equilibrium value was shown to develop already during the early stage of terrace formation.[13] On a longer time scale (compared to scales of intrachain dynamics) the pattern of terraces is still coarsening. This proceeds due to the effective line tension of the two-dimensional islands (holes) which tends to minimize the total length of the terrace edges with time. However, on a smaller length scale (a few microdomain spacings) during the late stages of terrace formation the film thickness and the step profile can be considered

* Corresponding authors. E-mail: larisa.tsarkova@uni-bayreuth.de, a.sevink@chem.leidenuniv.nl, and avzvelindovsky@uclan.ac.uk.

† Present address: IBM Research GmbH, Sumerstrasse 4, CH-8803 Rüschlikon, Switzerland.

10.1021/ma071107a CCC: $37.00
Published on Web 08/21/2007

constant. An extended summary of these studies can be found in recent reviews.[5,14−16]

It is now well-established that a cylinder-forming block copolymer under confinement and strong surface fields forms microstructures that deviate from that of the corresponding bulk material. Surface structures like lamella (L), perforated lamella (PL), perpendicular cylinders ($C_\perp$), cylinders with necks ($C_\parallel C_\perp$), and spheres on a top of a perforated lamella (PL-S) are examples of simulated[17−19] and experimentally observed morphologies[20−26] that are formed in thin films of bulk cylinder-forming block copolymers. While the equilibrium structures in thin films of block copolymer have widely been investigated, the dynamics of nanostructured fluids in thin films are an issue of a recent interest.[27,28]

The modeling part of this paper was inspired by unique in-situ SFM measurements of terrace formation, where both the macroscale development of the thickness gradient and the related microscale phase transitions were resolved. The calculational method based on the dynamic self-consistent field theory (DSCFT), originally proposed by Fraaije,[29] has been previously used to model the pattern formation in confined environment. The calculations matched the SFM experiments in great detail. Moreover, the theoretical approach provides decisive understanding of the experimental results as it allows more extensive variation of the system parameters than one could achieve in experiments. In our earlier work we identified deviations from the cylinder bulk morphology as surface reconstructions[24] and constructed phase diagrams which allow to distinguish between surface field and confinement effects.[18,19,24] Further, in recent study we found that the *dynamics* of elementary structural transition in experiment and simulation well accord. We demonstrated that DSCFT describes the microdomain dynamics on long time scales in great detail.[27] Furthermore, quantitative analysis of defect motion led to an estimate of the interfacial energy between the cylinder and the PL phases.

In our previous work[30] we have introduced a DSCFT-based model of a block copolymer film with a free surface and considered the dynamics of terrace development. Here, we rationalize the parametrization choice of this earlier study and focus on a detailed quantitative comparison of the early stage of terrace formation with the actual experiment. The paper is organized as follows: First, we introduce the computational model of free surface and related parameters. Next we describe continuous in-situ SFM measurements of the dynamics of the surface relief structures and phase transitions in thin triblock copolymer film under solvent annealing. Then we present the results of the parametrization of the model system aiming to match the experimentally observed structures. Finally, we analyze and compare the development of the thickness variation (terrace formation) and the related phase transitions in computational simulation and in in-situ experiment and discuss the underlying mechanisms.

2. Method

2.1. Theoretical Model. The mesoscopic DSCFT employs a coarse-grained field description of the polymer system. The free energy, however, is based on a microscopic Hamiltonian and therefore explicitly incorporates the specificity of the polymer chain. Furthermore, we use a separation of scales and consider a time scale at which, for given fields, the polymer chains are fully relaxed. The field dynamics is then given by a standard set of stochastic Langevin equations, where the stochastic terms represent mesoscopic fluctuations, according to the fluctuation−dissipation theorem. An overview, and details of this type of method, can be found in refs 29 and 31. The chain conformations at each point in time are specified by fields, and the dynamic equations for the fields describe the collective diffusive dynamics of the polymer system; hydrodynamic effects are neglegted. We remark that hydrodynamic phenomena are known to play only a minor role in the evolution of many systems, in particular in dense block copolymer systems.

In the following we shortly review the DSCFT that was also used in our earlier experimental/computational studies[24,27,30,45] and discuss the coarse-grained variables and parameters we have chosen for the model.

Molecular Model and the Free Energy Functional. An ideal Gaussian chain is used as molecular model in the microscopic Hamiltonian. The chemical composition of the polymer molecule is reflected by beads of different types, labeled by the index I. On a coarse-grained level, the microstructure patterns of polymeric systems are described by the density fields $\rho_I(\mathbf{r})$. We consider a system of volume V which contains n molecules of the length N. The free energy for such a system can be expressed as

$$F[\rho] = -kT \ln \Psi^n/n! - \sum_I \int_V U_I(\mathbf{r})\, \rho_I(\mathbf{r})\, \mathrm{d}\mathbf{r} + F^{\mathrm{nid}}[\rho] \qquad (1)$$

Here Ψ is the partition function for the ideal Gaussian chain of the length N in the external fields U_I. The external potentials U_I and the density fields ρ_I are bijectively related[32] in a self-consistent way via a density functional for the Gaussian chain.[33] F^{nid} is the contribution due to the nonideal mean-field interactions. For the cohesive interaction between the beads a Gaussian kernel is used:

$$\epsilon_{IJ}(\mathbf{r} - \mathbf{r}') \equiv \varepsilon_{IJ}^0 \left(\frac{3}{2\pi a^2}\right)^{3/2} \mathrm{e}^{-3(\mathbf{r}-\mathbf{r}')^2/2a^2}$$

The strength of the interaction, ε_{IJ}^0 (in kJ/mol), is directly related to the Flory−Huggins parameter ($\chi_{IJ} = 1000\varepsilon_{IJ}^0/N_a kT$). The input to the free energy functional is

$$F^{\mathrm{coh}}[\rho] = \frac{1}{2}\sum_{I,J} \int_V \int_V \epsilon_{IJ}(\mathbf{r} - \mathbf{r}')\, \rho_I(\mathbf{r})\, \rho_J(\mathbf{r}')\, \mathrm{d}\mathbf{r}\, \mathrm{d}\mathbf{r}' \qquad (2)$$

The compressibility of the system is included via

$$F^{\mathrm{e}}[\rho] = \frac{k_{\mathrm{H}}}{2} \int_V \Big(\sum_I \nu_I(\rho_I(\mathbf{r}) - \rho_I^0)\Big)^2\, \mathrm{d}\mathbf{r} \qquad (3)$$

Here k_{H} is Helfand coefficient, ρ_I^0 is the average concentration of the component I, and ν_I is the bead volume.

Solid Substrate. The solid surfaces are treated like hard walls, also called "mask fields", which constrain a thin film by keeping the flux perpendicular to the substrate equal zero.[34,35] In the unconstrained directions, periodic boundary conditions are used. The interactions with the masks are taken into account in the same way as the interaction between the beads. The surface field induced term in F^{nid} is

$$F^{\mathrm{surf}}[\rho] = \frac{1}{2}\sum_\alpha \sum_I \int_V \int_V \epsilon_{IM_\alpha}(|\mathbf{r} - \mathbf{r}'|)\, \rho_I(\mathbf{r})\, \rho_{M_\alpha}(\mathbf{r}')\, \mathrm{d}\mathbf{r}\, \mathrm{d}\mathbf{r}' \qquad (4)$$

where $\rho_{M_\alpha}(\mathbf{r}')$ describes the position of the mask ($\rho_{M_\alpha}(\mathbf{r}')$ is equal to 1 if $\mathbf{r}'$ belongs to the mask or 0 if $\mathbf{r}'$ belongs to the polymer film).

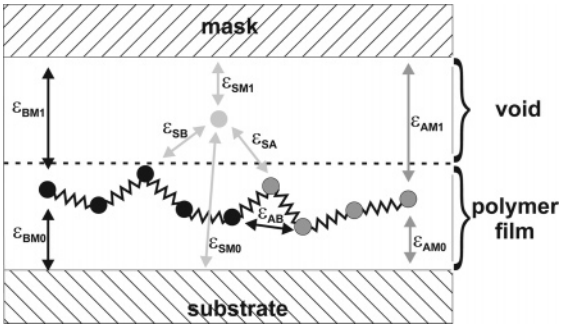

Figure 1. Schematic representation of the simulation setup. The corresponding interactions between system components are indicated by arrows. Block copolymer molecule is represented by the beads-and-springs model. An A_4B_5 molecule is shown for simplicity.

Free Surface. The free surface is created via introducing a void component. The void component is treated as a single-bead bad solvent.[30,36] Initially, the block copolymer film is macroscopically phase separated from the void component. The interactions with this void component are taken into account in the same way as the interaction between the polymer beads (via additional interaction parameters ε_{IS}).

Input Configuration. The numerical schemes explicitly consider the external potential fields U_I[33] instead of the density fields. Therefore, the input densities ρ_I^{input} cannot be imported directly. They are generated by iterative optimization of $U_I(\mathbf{r})$ with initial values $U_I(\mathbf{r}) = 0$ prior to the application of the dynamic scheme. An update of the external potentials is accepted when the difference between the input densities ρ_I^{input} and $\rho_I(U_I)$ is smaller than some preset value $\delta \ll 1$.

Dynamic Equations. The thermodynamic forces that drive the phase separation and the structure formation are local gradients in the intrinsic chemical potential. The chemical potentials are derived from the functional differentiation of the free energy

$$\mu_I(\mathbf{r}) = \frac{\delta F}{\delta \rho_I(\mathbf{r})} \tag{5}$$

We assume a diffusive dynamics of the density fields and solve the Langevin diffusion equations numerically:

$$\frac{\partial \rho_I}{\partial t} = M_I \nabla \cdot \rho_I \nabla \mu_I + \eta_I \tag{6}$$

where M_I is a constant mobility of bead I (diffusion coefficient) and η_I is a thermal noise, distributed according to the fluctuation−dissipation theorem.

2.2. Simulation Parameters of the Free Surface Model. General Considerations. To model the behavior of supported block copolymer films, we use the following starting configuration. Two masks M_0 and M_1 confine the simulation box from top and from bottom, respectively. The lower half of the box is occupied by the block copolymer film, while the upper half is the void component. Initially, the copolymer film is flat. The boundary between the void phase and the polymer film corresponds to a free surface and is expected to show undulation instabilities.[36] The model system is schematically represented in Figure 1. The simulation parameters of choice are the initial height of the film and the pairwise interaction parameters (see Figure 1). There are altogether nine interaction parameters: the interaction parameter between the polymer beads ε_{AB}, the interaction parameters of the polymer beads with the void component ε_{AS} and ε_{BS}, the interaction parameters of the polymer beads with the lower (ε_{AM_0} and ε_{BM_0}) and with the upper mask (ε_{AM_1}, ε_{BM_1}), and the interactions between the void component and the two masks (ε_{SM_0}, ε_{SM_1}). In the following part we describe the determined choice of each parameter.

Table 1. Structure Notation

structure	notation
perpendicular cylinders	$C_\perp$
short perpendicular cylinders, spheres	S
one layer of parallel cylinders	$C_{\parallel,1}$
two layers of parallel cylinders	$C_{\parallel,2}$
three layers of parallel cylinders	$C_{\parallel,3}$
parallel cylinders with necks to the polymer−air interface	$C_\parallel C_\perp$
parallel cylinders with necks to the substrate	$C_\perp C_\parallel$
wetting layer	W
perforated lamellae	PL
lamellae	L
coexistence of structures in one layer	*/*
coexistence of separate layers with different structures	*−*

Molecular Model. Both the Gaussian chain topology ($A_3B_{12}A_3$) and the interaction parameter between the polymer beads ε_{AB} (6.5 kJ/mol) are the same as in our earlier comparative theoretical[18,19,30] and experimental studies.[24,25,27]

Interaction of the Polymer Beads with the Substrate. In the earlier works[18,24] on thin films we have shown that the calculated structures with the effective surface interaction $\varepsilon_M = \varepsilon_{AM_0} - \varepsilon_{BM_0}$ of 6−7 kJ/mol match in great detail the experimentally observed structures.

Interaction of the Polymer Beads with the Void Component. The values of ε_{AS} and ε_{BS} determine the interaction of the polymer beads with the void component and are analogous to the surface tension of the block copolymer components in experiments. They can be calculated directly from the surface tension values of the polymers.[37−39] However, because of the extra constraints resulting from the periodic boundary conditions, this approach is not effective, as was shown in our previous publication.[30] Therefore, we determine the values of ε_{AS} and ε_{BS} by a parametrization procedure (see section 3.2). As a starting point, we assume the difference $\varepsilon_{AS} - \varepsilon_{BS}$ to be similar to the effective surface interaction in a slit (6−7 kJ/mol).[18]

Simulation Box. We set the initial thickness to the incommensurable situation corresponding to 1.5 layers of cylinders, analogous to the experiment. The height of the simulation box is set to be twice the film thickness, and additionally, two grid units are occupied by the mask fields. Lateral dimensions of 128×32 grid units are chosen to keep the computational time within reasonable limits.

Film Setup. In order to avoid floatening of the film from the substrate, we set the void−upper mask M_1 interaction to a negative value (attractive) and the void−bottom mask M_0 interaction to a positive value (repulsive). Additionally, the polymer beads are repelled from the upper mask. For this purpose we set $\varepsilon_{SM_1} = -4$ kJ/mol and $\varepsilon_{AM_1} = \varepsilon_{BM_1} = \varepsilon_{SM_0} = 8$ kJ/mol.

Time Scale. In our previous paper,[27] one simulation step was calculated to be about 6 s of the experimental measurement time. We assume the time scaling to be of the same order of magnitude in the present setup with the void component. Under this assumption, calculations over 30 000 time steps are comparable to an experimental annealing of the SBS film for several hours, when well-developed terraces are observed.

Notation. Structure notations used in the present study are similar to that in our previous works[30] and are summarized in Table 1.

2.3. Experiment. Sample Preparation. As an experimental reference system we studied a thin film of a polystyrene-*block*-polybutadiene-*block*-polystyrene (SBS) triblock copolymer (from Polymer Source Inc.) with weight-averaged molecular weights of the polystyrene (PS) blocks of $M_{W,PS} = 14$ kg/mol and $M_{W,PS} = 15$ kg/mol and of the polybutadiene (PB) block of $M_{W,PB} =$

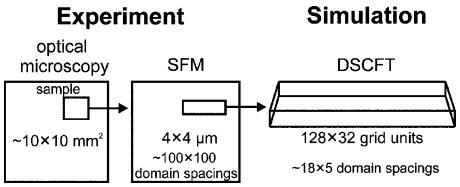

Figure 2. Schematic comparison of typical lateral scales that are covered in experimental measurements (optical microscopy and surface force microscopy) and in our simulation box.

73 kg/mol. The glass-transition temperatures of the respective homopolymers range from −83 to −107 °C for PB and from 80 to 100 °C for PS.[40] The surface tension of PB, $\gamma_{PB} = 31$ mN/m, is considerably smaller than the surface tension of PS, $\gamma_{PS} = 41$ mN/m.[40] A 70 ± 2 nm thick film was spin-cast from a toluene solution onto a silicon substrate. The sample was placed in a fluid cell of a Multimode SFM (Digital Instruments, Veeco Group) and exposed to a controlled chloroform vapor.[25] The chloroform vapor pressure was adjusted to set the polymer volume concentration in the film to $\phi = 0.73$. In bulk, at this concentration SBS forms cylinders with a characteristic spacing of 39.0 ± 0.5 nm.[25]

SFM Imaging and Movie. The changes in the surface topography and in the microdomain structure have been followed with in-situ scanning force microscopy (SFM) using standard silicon cantilevers (with a resonance frequency of 300 kHz; Nanosensors) in tapping mode. Light tapping conditions resulted in a phase contrast of 2°. The acquisition rate for a 4 × 4 μm^2 image (512 × 512 pixels) was 2.5 min per image. The resulting SFM images were flattened, registered, corrected for image distortion, and compiled into an SFM movie[41] using a homemade software. Because of a rather large thermal drift, the analysis of the same spot of the sample is possible only by picking a small area of one frame and tracking it into earlier and later frames. The movie[41] covers 6.75 h of annealing the SBS film under controlled vapor pressure and captures the early stage of terrace formation. For further experimental details see refs 13, 25, and 27.

Comparative Dimensions. Figure 2 compares the sample dimensions of the experiment with that of the computational simulation. In experiments a typical film surface area available for the optical microscopy or SFM measurements is about a cm^2 with an averaged terrace size of about several μm^2. In SBS films, each terrace accommodates in the lateral direction up to several hundred microdomains.

3. Results

3.1. Film Evolution in Experiment. The detailed phase behavior in SBS films after annealing in a neutral solvent has recently been studied at varied thickness and polymer content in a swollen film.[25] The initial dry film thickness (~70 nm) and annealing vapor pressure were chosen in accordance with the phase diagram of this polymer such as to make the thickness of the swollen film (at polymer volume fraction $\phi_p = 0.73$) equal to 1.5 layers of cylindrical structures. These films of incommensurable thickness are not stable upon annealing and form terraces with one and two layers of structures. As it was shown earlier in ref 25, the PL structure is expected within the lower terrace, while the second terrace shows a cylindrical structure ($C_{||,2}$). Perpendicular cylinders ($C_\perp$) are stabilized at the transition region between these terraces.

In the dynamic measurements described below, we start with the initially smooth spin-coated film. The associated microstructure (a random coexistence of white stripes, lying polystyrene cylinders $C_{||}$ and white dots without a long-range order, presumably perpendicular cylinders $C_\perp$[25]) is formed during the spin-coating procedure by the fast removal of the solvent. The initial stage of the surface-relief-structure development upon annealing was imaged with in-situ SFM, and the data were processed into a SFM movie.[41] Below we describe in detail the observed evolution of the local thickness gradient (terrace formation) and the accompanying phase transitions.

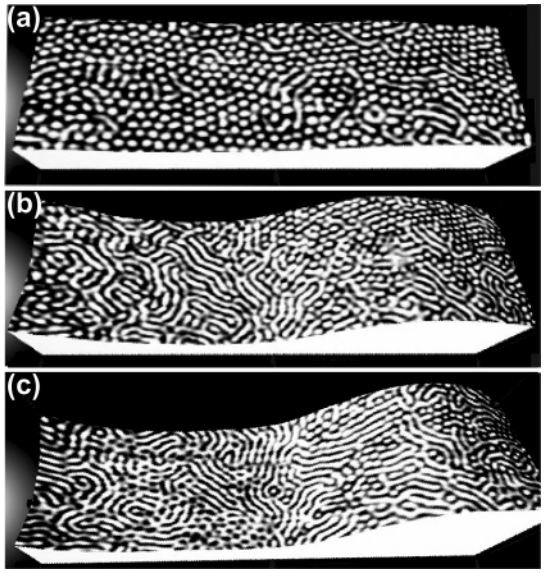

Figure 3. Snapshots of the in-situ SFM movie (0.675 × 2.625 μm) illustrating the dynamics of terrace formation at (a) 0.5, (b) 4, and (c) 6.75 h of annealing in solvent vapor. 3D pictures are constructed by using the height image as a topography and the phase image as a texture. White stripes and white dots are associated with polystyrene lying and perpendicular cylinders, respectively, while black dots in (c) correspond to the butadiene-filled perforations in a polystyrene sheet. The SFM movie can be found in the Supporting Information.[41]

Figure 3 displays the SFM movie snapshots which correspond to 0.5 h (a), 4 h (b), and 6.75 h (c) of annealing. At the initial stage of annealing the swollen SBS film already shows a slight height modulation (Figure 3a). As can be followed in the SFM movie,[41] the microstructure development proceeds first via ordering of dots into a hexagonally ordered pattern. During the time interval between 3 and 5 h the bright PS dots rearrange into bright PS stripes ($C_{||}$) within the lower terrace (see Figure 3b). Afterward, the PS-rich cylinders transform into PL (dark dots in bright matrix) (Figure 3c). The $C_{||}$ to PL phase transition takes about 10 h and has been described recently in great detail for constrained film thickness.[27] Here we focus on the first 7 h of the structure development upon annealing, where the thickness gradient develops gradually and the step height reaches about 80% of its equilibrium value.

It should be noted that the interpretation of the structures in the SFM phase images cannot be done unequivocal. In particular, the bright dots can be associated with the $C_\perp$ structure, as well as with the hybrid structures, such as $C_{||}C_\perp$ with the necks facing the free surface. Structure information provided by the SFM technique is limited to information of the upper film layer. Computational modeling, however, provides direct structural information throughout the polymer film and thereby complements and extends the SFM experiment. On the other side, the experimental data can be used to coordinate and parametrize the theoretical model. Moreover, searching in the parameter space allows to study the effect of the system parameters at a much wider range than is typically available in experiments.

Table 2. Parameter Sets of Simulations

run	ε_{SA}, kJ/mol	ε_{SB}, kJ/mol	ε_{AM_0}, kJ/mol	ε_{BM_0}, kJ/mol	H grid units
A	17	10	3	−4	9
B	16	10	2	−4	9
C	16	9.5	3	−4.5	9
D	16	9.5	12	0	9
E	16	9.5	0	3	12

3.2. Simulation Setup vs Experiment. We performed a number of simulation runs in order to match the structures and transitions observed in the experiment.[41] In particular, we varied the interaction of the blocks with the surface and with the void component. The choice of the parameter range is based on the considerations presented earlier in the parametrization section 2. The studied systems are summarized in Table 2.

Figure 4b presents a structure analysis of the calculation results after 30 000 time steps for these particular systems. For comparison, we have included data for a wedge-shaped slit (symmetric case $\varepsilon_M = 6$, first column in Figure 4b),[18] which we had found to match the equilibrium behavior of SBS films in great detail.[24] In these simulations, a thickness gradient is imposed and the structure adjusts to this varying height. For the parameter set A (Table 2) the void/polymer interface (the free surface of the film) remains flat after 30 000 time steps. $C_{||}C_{\perp}$ structures are stable for this thickness. For the slit system an equivalent surface structure ($C_{\perp}$) is found for this particular film thickness. At a slightly reduced interaction of the bead A with the void component ($\varepsilon_{SA} = 16$ instead of 17) and with the substrate ($\varepsilon_{AM_0} = 2$ instead of 3) (parameter set B) the film shows pronounced surface roughening. A depression associated with one layer of parallel cylinders ($C_{||,1}$) is formed in the middle of the simulation box. For the other thicknesses in the box the $C_{||}C_{\perp}$ is found. In the parameter set C (Table 2) the selectivity of the surface and of the substrate to the blocks are slightly increased, still yielding the structures similar to that in system B. However, the formation of a second layer of cylinders is promoted by the joining necks (Figure 4c, parameter set C). Additionally, defects appear in the lower terrace. These T-junctions are known to serve as nucleation centers for the PL phase.[27]

For the parameter set D (where the surface field value $\varepsilon_{AM_0} - \varepsilon_{BM_0}$ is increased) the free surface of the film also shows roughening. At the lowest thickness a $C_{||,1}$ structure appears. At intermediate thickness, the film shows a mixture of $C_{||}C_{\perp}$ and of one layer of a perforated lamella with weakly segregated drops on top of it (PL-S). At the largest thickness, a small amount of $C_{||,2}$ develops.

Although systems B to D reproduce the experimental results reasonably well (Figure 4c), the structures formed in the case of the parameter set C after 30 000 time steps fit the experimental heights and the slope structures (Figure 4a) the best. Moreover, the parameter set C is comparable to the matching simulation in the earlier slit study.[24]

Earlier, height measurements in SBS films suggested an additional layer of material underneath the film, which corroborated the existence of a wetting layer everywhere at the film−substrate interface.[25] Further development of the computational model was done by introducing a wetting layer next to the substrate (parameter set E). The interactions with the void component are the same as in the system C. The interactions with the substrate are set to $\varepsilon_{MA} = 0$ and $\varepsilon_{MB} = 3$ in order to get wetting layer.[18] In addition, the initial height of the polymer film is increased to 12 grid units (box size $128 \times 32 \times 26$). Because of the wetting layer, this initial thickness corresponds to 1.5 layers of cylinders. System E shows structures similar to the system C in the presence of an A-rich wetting layer. The comparison of these two systems provides insight into the possible role of the wetting layer on structure formation and microdomain dynamics. In the remainder we refer to the calculation with parameter set C as "the simulation without wetting layer" and the simulation with parameter set E as "the simulation with wetting layer".

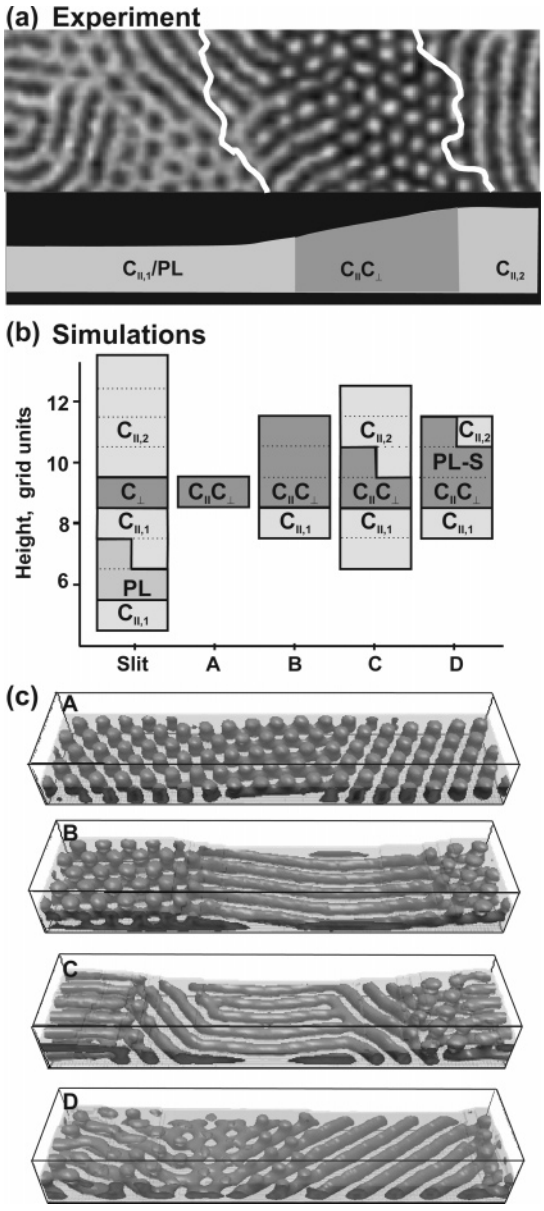

Figure 4. (a) SFM phase image of a slope between the first and the second terraces in SBS film which have been equilibrated in the solvent vapor for 7 h.[24] The sketch below the image illustrates the observed sequence of the morphologies at the commensurable and intermediate thicknesses. (b) Calculated diagram of the system structure vs height (thickness) for the systems A-D (Table 2) after 30 000 time steps. The system in a slit from ref 18 is shown as a reference only. (c) Simulated structures for the systems A−D shown in (b). Gray structure is the A component (isodensity level $\rho_A = 0.42$); transparent gray volume indicates the film topography (isodensity level of polymer is larger than 0.9).

3.3. Film Evolution in Simulation. Both systems were simulated up to 100 000 time steps. Within the first 200−1000 time steps, the formation of A- and B-rich layers is initiated by the solid surface in the initially flat and homogeneous film. Next, the in-plane separation takes place. In the system without wetting layer the film forms parallel cylinders near the substrate and droplets of the A-rich phase next to the free surface. The droplets connect with cylinders, and thus a transition to $C_{||}C_{\perp}$ takes place.

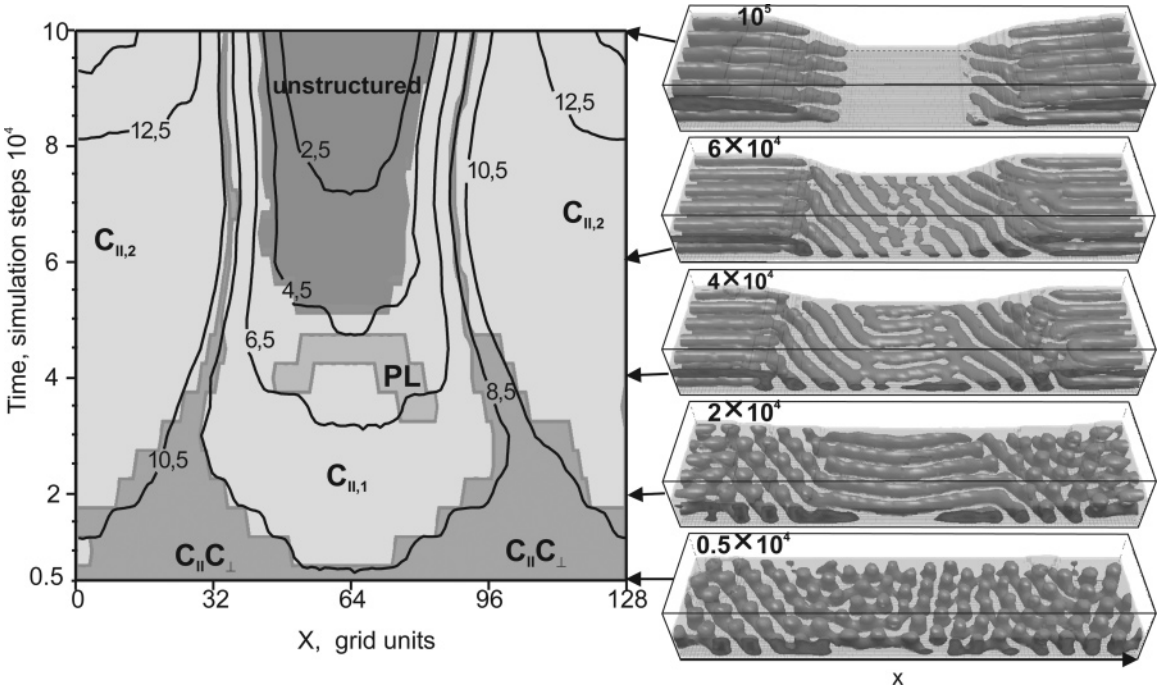

Figure 5. Graphic representation of the film structure and corresponding heights as a function of time for the system without wetting layer. Different tints of gray correspond to indicated structures; the black lines are the isoheight lines. Right-hand pictures are representative examples of simulation snapshots as indicated by arrows. The movie[42] can be found in the Supporting Information.

In the system with the wetting layer the A component preferentially covers the surface, causing an unstructured wetting layer. The two layers above this wetting layer interconnect and form $C_{\perp}$, rather than $C_{II}C_{\perp}$ as in the system without wetting layer. Since the dynamics of structure formation immediately after microphase separation cannot be compared with our in-situ SFM experiment, where the structure is affected by the spin-coating process, we will not focus on the very first stages (below 5000 time steps). We note that the early stage of structure formation has been recently described for a system analogous to the system D (Table 2).[30]

Simulation without Wetting Layer. The dynamics of thickness gradient formation and structure development for the system C is captured as a movie[42] and analyzed in Figure 5. The simulated structures and heights are analyzed from the same region in the middle and along the longest axis of the simulation box each 5000 steps. Gray levels indicate different structures. The borders between the structures are determined by visual analysis and therefore are drawn arbitrarily. As a reference we also present isoheight[43] lines (in black). Examples of the structural evolution are shown as simulation snapshots at the indicated time steps.

With time, the amplitude of the thickness fluctuations becomes sufficient to induce terrace formation. After 8000−9000 time steps we observe in the thinnest region a structural transition to one layer of cylinders. In the regions with higher film thickness after 20 000 time steps two layers of parallel cylinders are formed. Together with a small decrease of the film thickness, the PL phase appears at the lower terrace of the film (after 40 000 time steps). As the thickness of the lower terrace decreases further, the PL phase first changes to one layer of defect-free cylinders and later to a disordered layer. The height lines on the graph (Figure 5) accord with the contour lines of the phase regions. The approximate borders are 10.5 grid units for the transition between $C_{II,2}$ and $C_{II}C_{\perp}$, 8.5 grid units for $C_{II}C_{\perp}$ to $C_{II,1}$, and 4.5 grid units for the $C_{II,1}$ to disordered phase. The structures below 4.5 grid units can be divided into two regions. Between 4.5 and 2.5 grids the film is unstructured (phase-separated material with no symmetry), and below 2.5 grids the system is disordered/mixed. The PL structure and the $C_{II,1}$ structure coexist at a certain film thicknesses and time conditions, like in the experiment.

Simulation with Wetting Layer. Generally, transitions in the system with wetting layer (asymmetric wetting conditions) are similar to the system described above (see ref 44). However, in the presence of the wetting layer, the $C_{\perp}$ structure is formed initially, in contrast to the $C_{II}C_{\perp}$ structure in the system without wetting layer. Indeed, after the transition to $C_{II,1}$ in the lower terrace has taken place, the remaining $C_{\perp}$ interconnect to form $C_{II}C_{\perp}$ structures. When increasing the local thickness after 30 000 time steps the $C_{II}C_{\perp}$ changes to $C_{II,2}$. At the same time the order of the cylinders in the thinner part of the film (in the first terrace) is improved. As the difference in local heights increases, necks start to form on the top of $C_{II,2}$, indicating a transition to $C_{II,3}$ (90 000 time steps). The $C_{II,1}$ phase becomes thinner and less phase separated. Importantly, the PL phase was not observed. This result is in a good agreement with the experiments on thin films of SB diblock copolymer, which is a structural analogue of SBS triblock copolymer. In this study the PL phase was stabilized under symmetric wetting conditions and was not observed in SB films with a wetting layer.[26]

4. Discussion

We focus on the evolution of local morphology and its relationship to thickness and terrace formation in block copolymer films of incommensurate height. The time-elapsed SFM measurements are compared to the numerical modeling using DSCFT. It should be noted that the latter approach does not directly explore the microscopic dynamics of chain motion. As mentioned before, DSCFT rather describes the evolution of density fields, under the conditions that diffusion/relaxation of single (coarse-grained) chains within the field is rapid compared to the coordinated motion of many chains. The good match between the film development in simulations and in the experimental annealing suggests that the kinetic model in DSCFT is applicable. In particular, on time scales beyond single chain relaxation, where this coarse-grained approach is valid, this model adequately describes the microdomain dynamics in

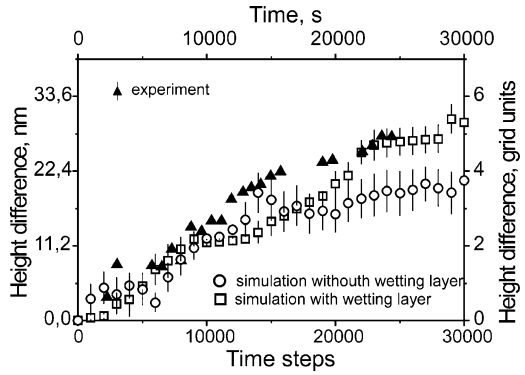

Figure 6. Difference between the maximum and the minimum heights on the free surface in simulations [open symbols] (right-hand axis) and in experiment [black triangles] (left-hand axis) plotted as a function of the simulation time (bottom axis) and annealing time (top axis), respectively.

the experimental system. Moreover, the computational method allows for a time-resolved study of the morphology of the film beyond the surface layer to which the experimental studies are limited.

4.1. Comparison of Simulation and Experiment. 4.1.1. Dynamics of Surface Relief Structures. Both in experiment and in simulations, the structural transition is accompanied by a change in local height of the film. In Figure 6 we compare the step height, the difference between the maximum height on the top of the island and minimum height inside the hole, as a function of time in experiment and in simulations for the systems with and without wetting layer. At the early stage of terrace formation the two simulation systems show structural transitions similar to that in the experiment. The relation between the experimental heights and grid units was determined beforehand from the comparison of bulk spacings in experiment and in the calculation (1 grid unit corresponds to 5.6 nm).[18]

The time axis was scaled by matching the simulation and the experimental graphs. The best fit is found for 1 computational time step = 0.8−1 s of real experimental time (on the graph we use 1 step equaling 1 s). Our comparison merely focuses on the early stage of terrace formation where phase transitions are the same in the experiment and in the simulations.

The results of structure calculation are shown after 5000 and 25 000 time steps in Figure 7a,b in a form of surface structures imaged with SFM.[30] In Figure 7c the same spot on the slope between the neighboring terraces in the experimental system is shown after 0.5 and 6.75 h of annealing. The height difference after 6.75 h of annealing is ∼27 nm, corresponding to about 80% of the equilibrium step height. Along the pathway the initial bright dots transform to bright stripes and small patches of dark dots at thinner regions. They can be interpreted as a PL phase.[24] At intermediate thickness, bright dots are the dominating structures. At the largest thickness white stripes are formed. The comparison of surface structures in Figure 7a−c suggests that the initial white-dots pattern and the dots-and-stripes pattern after 25 000 time steps in the simulations (see Figure 7a,b) are similar to the experimental images after 0.5 and 6.75 h of vapor treatment (Figure 7c).

The dots-to-stripes transition represents the transition from $C_\perp$ and $C_{||}C_\perp$ to $C_{||,1}$ in the lower terrace or to $C_{||,2}$ in the upper terrace. The details of these transitions in the experiment and in the simulations are considered below.

4.1.2. $C_\perp/C_{||}C_\perp$-to-$C_{||,1}$ Transition. The pathway of the experimental dots-to-stripes transition in the lower terrace is

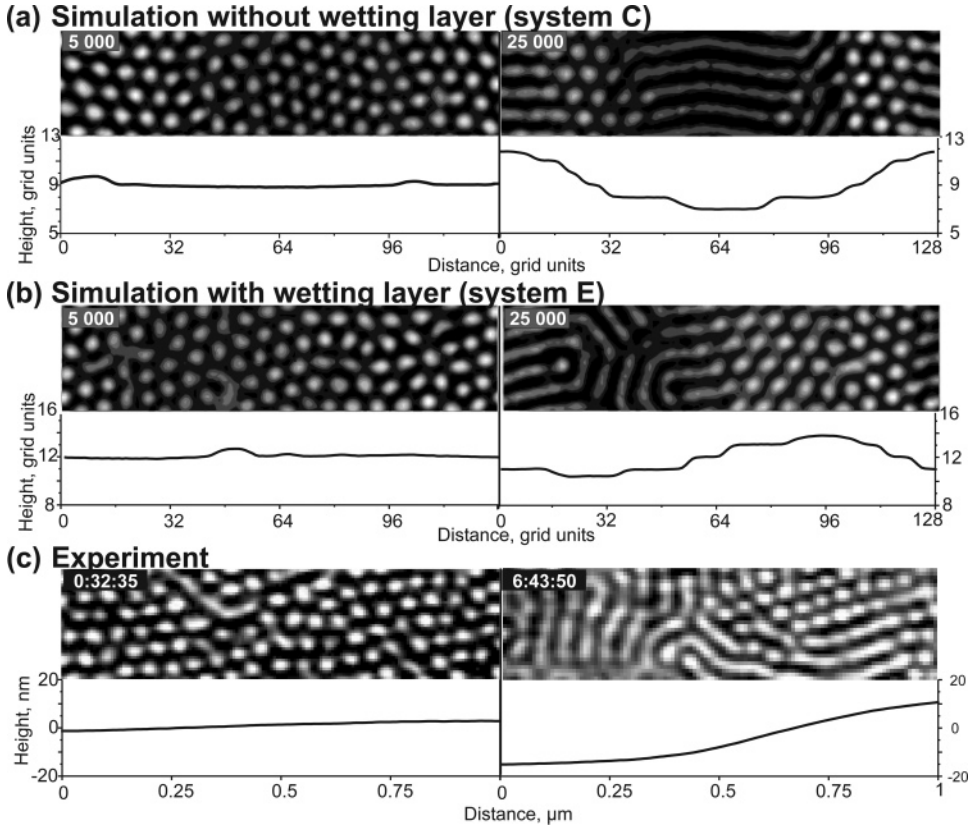

Figure 7. Simulation snapshots showing system C (a) and system E (b) from Table 2 at indicated time steps. The surface structures are calculated as the avarege density of the A component over the top two layers. Plotted heights are determined as described in ref 43. (c) Snapshots from the SFM movie showing the surface structures (phase image of tapping mode SFM) and surface topography of the same spot on the terrace slope at indicated annealing time.

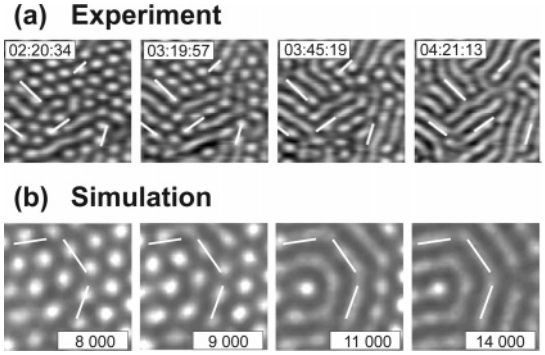

Figure 8. (a) Experimental snapshots at indicated times of solvent vapor annealing showing the dots-to-stripes phase transition. (b) Simulation snapshots of the surface structures (see Figure 7) for the system with wetting layer from Figure 6 showing the $C_\perp$-to-$C_{||}$ phase transition. The time steps are indicated at the bottom of the images. In (a) and (b) white bars are drawn parallel to the cylinders in the last image of each sequence and are superimposed onto the earlier images as a guide to eye to illustrate the structure development.

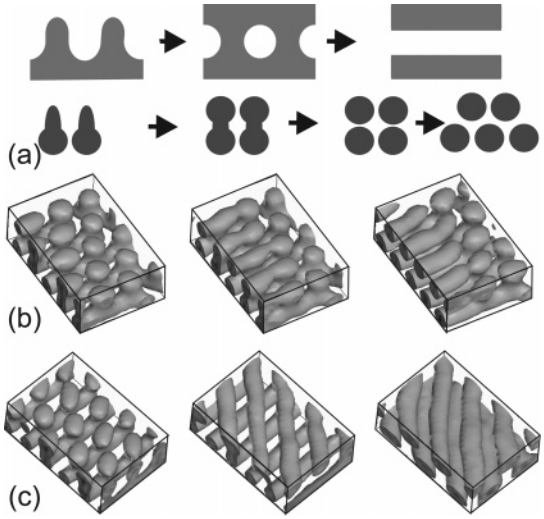

Figure 9. (a) Schematic representation of the $C_{||}/C_\perp$-to-$C_{||,2}$ transition shown as a side view (top row) and as a front view (bottom row). (b) Simulation snapshots of the system C (Table 1) after 19 000, 22 000, and 30 000 time steps (from left to right). (c) Simulation snapshots of the system E (Table 1) after 43 600, 47 000, and 60 000 time steps (from left to right).

shown in Figure 8a. The details of the underlying structure transition away from the air−polymer interface can be extracted from the simulation results.

In the system without the wetting layer, the $C_{||}C_\perp$ transforms into modulated or elongated cylinders. A further decrease of the film thickness in the middle of the hole leads to the development of $C_{||,1}$. The distance between the lying cylinders in $C_{||}C_\perp$ and in $C_{||,1}$ is the same; therefore, large-scale reorientation is redundant for matching the natural lateral domain spacing. The spacing between the dots (necks) is about 15% larger ($^2/_{\sqrt{3}}a_0$) than the spacing of lying cylinders a_0 (due to the hexagonal packing).[23] The necks can form a perfect hexagonal matrix even if the underlying cylinders form separate grains which orient 60° (or 120°) to each other.

For the system with wetting layer the upright cylinders ($C_\perp$) first elongate in the plane of the film toward the neighboring cylinders and finally coalesce. They form lying cylinders either directly or via intermediate structure of modulated cylinders (cylinders with necks). The connection between $C_\perp$ cylinders initially appears preferentially at grain boundaries in the $C_\perp$ structure (or at defects) and serves as a nucleus of the new $C_{||,1}$ structure. The top view of this transition is shown in Figure 8b. Comparing the directions of the grains in the $C_{||}$ phase to the direction of the grains in the earlier $C_\perp$ phase, we detect a rotation of the cylinders. The whole grain of parallel cylinders rotate by an angle of ∼10°. The final grain size is typically no larger than 3−4 cylinder spacings.

We find that the initial structure ($C_\perp$ or $C_{||}C_\perp$) strongly influences the resulting $C_{||}$ phase. If the transition proceeds by interconnecting perpendicular cylinders, the spacing of the in-plane cylinders will only be $c_0 = {}^{\sqrt{3}}/_2 a_0$. The initial grains of the $C_{||}$ phase are therefore formed with an unfavorably reduced spacing of the cylinders. This affects the further growth of the $C_{||,1}$ phase. The $C_\perp$ structure cannot simply transform into the $C_{||}$ structure by interconnecting cylinders without inducing strain. Therefore, the transition is slow (compared to $C_{||}C_\perp$-to-$C_{||}$) and starts from several nuclei close to each other. The outcome is a much smaller grain size of the $C_{||}$ phase in comparison to the $C_\perp$ grain size before transition. The grains try to relax their spacing by rotating the cylinders in the plane of the film. The rotation in the system with wetting layer is similar to the mechanism observed in the experiment (Figure 8); therefore, we concluded that white dots in SFM images correspond to perpendicular oriented cylinders rather than to cylinders with necks.

The structural transition shown in Figure 8 takes place in about 2 h of the experimental time and in ∼6000 simulation steps. Therefore, the time scale is the same as the time scale obtained from terrace growth (1 simulation step ∼ 1 s of real time), showing good consistency with the dynamics of surface topography.

4.1.3. $C_\perp/C_{||}C_\perp$-to-$C_{||,2}$ Transition. Another type of dots-to-stripes transition is a transition to two layers of lying cylinders. In the simulation, the formation of the second layer proceeds only from the $C_{||}C_\perp$ phase. The schematic details of this transition are shown in Figure 9a. When the film height reaches 11 grid units (14 grid units in the system with wetting layer), the deformed necks interconnect and a ladderlike structure is formed (see the second sketch in Figure 9a). The interconnection of $C_{||}C_\perp$ to $C_{||,2}$ starts either parallel to the cylinders in the bottom layer (Figure 9b) or under an angle of 60° (Figure 9c). As the structure evolves, the connections between the necks can be broken and formed again. The lifespan of this process is 1000 simulation steps, which corresponds to 10 min of the experimental time. This meets the experimental observation of the same phenomena, where fluctuations are visible at successive SFM scans (which also takes some minutes between reconnections). Cylinders in the layers adjust their position in the space to achieve hexagonal packing. The transformation requires translational (Figure 9b) or rotational (Figure 9c) rearrangement of cylinders on a large scale. In the example shown in Figure 9c the reorientation takes place via formation of a transient perforated lamella phase.[45]

At the late stage of the terrace development the $C_\perp$ structure has disappeared, and the $C_{||}C_\perp$ persists only at the intermediate thicknesses between one and two layers of cylinders.

4.2. Mechanisms of Transitions, Early and Late Stages. It was experimentally demonstrated that the behavior of supported thin films of block copolymers involves multiple time and length scales. On the one hand, the microphase separation and structure formation in the block copolymer phase occur on a short time scale (typically seconds or minutes) and cover distances of some tens of nanometers.[45,46] Terrace formation is a much slower process (typically hours) involving material transport over micrometer range. In this work we focus on the early stage of terrace formation. In the studied cylinder-forming

systems this stage is associated with considerable development of the height difference (up to 80% of the equilibrium step height) and related structure transitions.

We observe a spontaneous splitting of the initially homogeneous film thickness into continuously developing terraces with different heights. Height change and structural transitions are inseparable. Moreover, the simulations-revealed pathways of the $C_{\perp}/C_{||}C_{\perp}$-to-$C_{||,2}$ and $C_{\perp}/C_{||}C_{\perp}$-to-$C_{||,1}$ transitions suggest the diffusion of block copolymer chains along the structure interface. Both in simulations and in experiment we distinguish phase transitions which occur at constant height: ($C_{||}$-to-PL and PL-to-$C_{||}$). The formation of an intermediate PL phase enhances the connectivity and enables the defect annihilation or reorientation of whole domains ($C_{||}$-to-PL-to-$C_{||}$).[45]

We conclude that in the early stage of terrace formation interconnected structures/defects in domain edges are of great importance. In contrast to lamella-forming block copolymers,[10] in cylinder-forming systems the $C_{||}C_{\perp}$ structures are natural channels for the material transport between the lower and the upper terraces.

The late stages of terrace formation have recently been investigated.[7,28,47] In particular, the kinetics of the late-stage islands growth was described as the Ostwald ripening process. Three mechanisms were suggested for the lamellar systems to describe the kinetics of surface relief development (the movement of individual islands):[7] diffusional movement of whole islands, tunneling of individual block copolymer chains between layers, and flow of individual chains through defects in the structure. It was concluded that the flow of block copolymer chains through the defect structures is the primary mechanism for the late stages of island development.[7] Recently, the material transport mechanisms between terraces in cylinder-forming block copolymer film were investigated theoretically and experimentally,[48] and the time dependence of the flow at later stages was found to be diffusion-like. For the systems studied here it was shown earlier that the terrace formation at later stage is dominated by coalescence of surface structures and microdomains ordering.[27]

Finally, we remark that the development of an ultrathin disordered layer in the simulation movie 2 (system C) at late time steps resembles the droplet formation (or authophobic dewetting). In experimental systems with high chain mobility undesired dewetting leads to the rupture of block copolymer films already at very short experimental time scales (few minutes of annealing). As a result, the formation of the equilibrium microstructures cannot be followed experimentally. To our knowledge, there are no published studies which compare the kinetics of the competitive dynamic processes (terrace formation and dewetting) in block copolymer films. We can only state that both the macrodomain spacings and the orientational order are affected by the shear fields in dewetting rims.[5,49] Understanding the film stability toward dewetting requires a detailed analysis of several factors, including surface tension and surface field strength. Since the definition of surface tension for nanopatterned surfaces is ambiguous, there is a severe lack of theoretical guidance. The parameter set in system C could serve as a starting point for a detailed computational study on film stability, which is beyond the scope of the present work.

5. Conclusions

We have studied terrace formation in a thin film of a cylinder-forming block copolymers by a computational DSCFT method and have compared the results with the dynamic SFM measurements of the SBS block copolymer thin films. The complex dynamics exhibited by this system enriches the fundamental understanding self-assembly in block copolymers, highlighting the special relationship between morphology and dynamic processes in thin films.

Apart from the introduction of a free surface via a void component (and relevant new parameters for the free surface interactions), we have chosen a simulational system equal to the one considered in earlier publications.[18,19,24,27] We have focused on the early stage of terrace formation, where 80% of height changes occur. On the very early stage, not accessible in the experiment, we observe microphase separation and structure formation in the block copolymer film. The formation of the microstructure starts at the substrate. Subsequently, the initially flat film develops terraces. Experimental and simulation results agree that the change of the local height is strongly connected to the changes in the local microstructure. The detailed pathways of the structural transitions, as revealed by simulations, suggest a diffusion of block copolymer chains along the microstructure interfaces and indicate an important role of $C_{||}C_{\perp}$ (necks) structure as material-transport-channel between neighboring terraces in thin cylinder-forming films.

Kinetics of both the terrace height growth and the structural transition was found to be quantitatively similar in experiment and in simulations; 1 time step equals 1 s. The accordance between the simulation and the experiment supports the assumption that the early stage of terrace formation is governed by diffusion.

Acknowledgment. This work was supported by the Deutsche Forschungsgemeinschaft (SFB 481, TP B7 and A9). A.H. thanks the support of the State of Bavaria (HWP-Program).

Supporting Information Available: SFM movie: in-situ tapping mode SFM movie showing the development of the surface topography and the microdomain structures at early stage of terrace formation in a swollen SBS film with a polymer volume fraction of $\phi = 0.73$. The SFM images were rendered into 3D pictures with Pov-RayTM. The SFM topography images were used as a height field, while the SFM phase signal is represented as a texture. Bright structures correspond to polystyrene component. The movie starts after 5 min of equilibration of the spin-coated SBS film in chloroform vapor pressure. The displayed area is ($2.625 \times 0.675 \times 0.06$) μm^3. The frame rate is 152 s/frame; total capture time is 6 h 45 min. *Simulational movie, system C*: computer simulation (DSCFT method) of the early stage of the surface topography and microstructure development in the system with parameter set C (Table 2). For each displayed time step, gray structures represent the microstructure A component (isodensity level $\rho_A = 0.42$). In addition, transparent gray volumes show the film topography (isodensity level of polymer is larger than 0.9). The structure evolution is plotted every 200th time step, for 100 000 time steps in total. The dimention of the simulation box is $128 \times 32 \times 20$ grid elements. *Simulational movie, system E*: detailed structural evolution obtained with the computational DSCFT method. The movie shows the early stage of the surface topography and microstructure development in the system with parameter set E (Table 2). Gray structures represent the A component (isodensity level $\rho_A = 0.42$); transparent gray volumes show the film topography (isodensity level of polymer is larger than 0.9). The structure evolution is plotted every 200th time step, for 100 000 time steps in total. The dimention of the simulation box is $128 \times 32 \times 26$ grid units. This material is available free of charge via the Internet at http://pubs.acs.org.

References and Notes

(1) Bates, F. S.; Fredrickson, G. H. *Annu. Rev. Phys. Chem.* **1990**, *41*, 525−557.
(2) Fredrickson, G. H. *Macromolecules* **1987**, *20*, 2535−2542.

(3) Anastasiadis, S. H.; Russell, T. P.; Satija, S. K.; Majkrzak, C. F. *Phys. Rev. Lett.* **1987**, *62*, 1852−1855.
(4) Fasolka, M. J.; Banerjee, P.; Mayes, A. M.; Pickett, G.; Balazs, A. C. *Macromolecules* **2000**, *33*, 5702−5712.
(5) Tsarkova, L. In *Nanostructured Soft Matter: Experiment, Theory, Simulation and Perspectives*; Zvelindovsky, A. V., Ed.; Springer Verlag: Heidelberg, 2007; pp 226−261.
(6) Peters, R. D.; Yang, X. M.; Nealey, P. F. *Macromolecules* **2002**, *35*, 1822−1834.
(7) Heier, J.; Kramer, E. J.; Groenewold, J.; Fredrickson, G. H. *Macromolecules* **2000**, *33*, 6060−6067.
(8) Heier, J.; Sivaniah, E.; Kramer, E. J. *Macromolecules* **1999**, *32*, 9007−9012.
(9) Liu, Y.; Zhao, W.; Zheng, X.; King, A.; Singh, A.; Rafailovich, M. H.; Sokolov, J.; Dai, K. H.; Kramer, E. J.; Schwarz, S. A.; Gebizlioglu, O.; Sinha, S. K. *Macromolecules* **1994**, *27*, 4000−4010.
(10) Carvalho, B. L.; Thomas, E. L. *Phys. Rev. Lett.* **1994**, *73*, 3321−3324.
(11) Menelle, A.; Russell, T. P.; Anastasiadis, S. H.; Satija, S. K.; Majkrzak, C. F. *Phys. Rev. Lett.* **1992**, *68*, 67−70.
(12) Maaloum, M.; Ausserre, D.; Chatenay, D.; Coulon, G.; Gallot, Y. *Phys. Rev. Lett.* **1992**, *68*, 1575−1578.
(13) Knoll, A. Ph.D. Thesis, Universität Bayreuth, Bayreuth, Germany, 2003.
(14) Segalman, R. A. *Mater. Sci. Eng., R* **2005**, *R48*, 191−226.
(15) Fasolka, M. J.; Mayes, A. M. *Ann. Rev. Mater. Res.* **2001**, *31*, 323−355.
(16) Green, P. F.; Limary, R. *Adv. Colloid Interface. Sci.* **2001**, *94*, 53−81.
(17) Huinink, H. P.; van Dijk, M. A.; Brokken-Zijp, J. C. M.; Sevink, G. J. A. *Macromolecules* **2001**, *34*, 5325−5330.
(18) Horvat, A.; Lyakhova, K. S.; Sevink, G. J. A.; Zvelindovsky, A. V.; Magerle, R. *J. Chem. Phys.* **2004**, *120*, 1117−1126.
(19) Lyakhova, K. S.; Sevink, G. J. A.; Zvelindovsky, A. V.; Horvat, A.; Magerle, R. *J. Chem. Phys.* **2004**, *120*, 1127−1137.
(20) Henkee, C. S.; Thomas, E. L.; Fetters, L. J. *J. Mater. Sci.* **1988**, *23*, 1685−1694.
(21) Radzilowski, L. H.; Carvalho, B. L.; Thomas, E. L. *J. Polym. Sci., Part B* **1996**, *34*, 3081−3093.
(22) Kim, G.; Libera, M. *Macromolecules* **1998**, *31*, 2569−2577; **1998**, *31*, 2670−2672.
(23) Konrad, M.; Knoll, A.; Krausch, G.; Magerle, R. *Macromolecules* **2000**, *33*, 5518−5523.
(24) Knoll, A.; Horvat, A.; Lyakhova, K. S.; Krausch, G.; Sevink, G. J. A.; Zvelindovsky, A. V.; Magerle, R. *Phys. Rev. Lett.* **2002**, *89*, 035501/1−4.
(25) Knoll, A.; Magerle, R.; Krausch, G. *J. Chem. Phys.* **2004**, *120*, 1105−1116.
(26) Tsarkova, L.; Knoll, A.; Krausch, G.; Magerle, R. *Macromolecules* **2006**, *39*, 3608−3615.
(27) Knoll, A.; Lyakhova, K. S.; Horvat, A.; Krausch, G.; Sevink, G. J. A.; Zvelindovsky, A. V.; Magerle, R. *Nat. Mater.* **2004**, *3*, 886−891.
(28) Segalman, R. A.; Schaefer, K. E.; Fredrickson, G. H.; Kramer, E.; Magonov, S. *Macromolecules* **2003**, *36*, 4498−4506.
(29) Fraaije, J. G. E. M. *J. Chem. Phys.* **1993**, *99*, 9202−9212.
(30) Lyakhova, K. S.; Horvat, A.; Zvelindovsky, A. V.; Sevink, G. J. A. *Langmuir* **2006**, *22*, 5848−5855.
(31) Fredrickson, G. H.; Ganesan, V.; Drolet, F. *Macromolecules* **2002**, *35*, 16−39.
(32) Mermin, N. D. *Phys. Rev.* **1965**, *137*, 1441.
(33) Fraaije, J. G. E. M.; van Vlimmeren, B. A. C.; Maurits, N. M.; Postma, M.; Evers, O. A.; Hoffmann, C.; Altevogt, P.; GoldbeckWood, G. *J. Chem. Phys.* **1997**, *106*, 4260−4269.
(34) Sevink, G. J. A.; Zvelindovsky, A. V.; van Vlimmeren, B. A. C.; Maurits, N. M.; Fraaije, J. G. E. M. *J. Chem. Phys.* **1999**, *110*, 2250−2256.
(35) Huinink, H. P.; Brokken-Zijp, J. C. M.; van Dijk, M. A.; Sevink, G. J. A. *J. Chem. Phys.* **2000**, *112*, 2452−2462.
(36) Morita, H.; Kawakatsu, T.; Doi, M. *Macromolecules* **2001**, *34*, 8777−8783.
(37) Helfand, E.; Tagami, Y. *J. Chem. Phys.* **1972**, *56*, 3592−3601.
(38) Broseta, D.; Fredrickson, G. H.; Helfand, E.; Leibler, L. *Macromolecules* **1990**, *23*, 132−139.
(39) Linse, P.; Hatton, T. A. *Langmuir* **1997**, *13*, 4066−4078.
(40) Brandrup, J.; Immergut, E. H.; Grulke, E. A. *Polymer Handbook*; Wiley: New York, 1989.
(41) See SFM movie in the Supporting Information.
(42) See simulational movie, system C, in the Supporting Information.
(43) The density field values are only known at the lattice positions (although the calculations themselves are not restricted to the lattice). And we have a steep density gradient between the void component and polymer film. The mixture of these two phases appear only on the boundary. We use the following definition for the interface between void and polymer: $H(x,y) = z - (\rho_S)/(\rho_A + \rho_B + \rho_S) \sim z - \rho_S$; here z is the height where the mixture of void and polymer appears. The height profiles for different y after 5000 simulation steps are similar; the calculated deviations were below 0.5 grid units.
(44) See simulational movie, system E, in the Supporting Information.
(45) Tsarkova, L.; Horvat, A.; Krausch, G.; Zvelindovsky, A. V.; Sevink, G. J. A.; Magerle, R. *Langmuir* **2006**, *22*, 8089−8095.
(46) Tsarkova, L.; Knoll, A.; Magerle, R. *Nano Lett.* **2006**, *6*, 1574−1577.
(47) Grim, P. C. M.; Nyrkova, I. A.; Semenov, A. N.; Tenbrinke, G.; Hadziioannou, G. *Macromolecules* **1995**, *28*, 7501−7513.
(48) Belyi, V.; Witten, T. *J. Chem. Phys.* **2004**, *120*, 5476−5485.
(49) Hahm, J.; Sibener, S. J. *Langmuir* **2000**, *16*, 4766−4769.

MA071107A